J. metamorphic Geol., 2010, **28,** 509–526 doi:10.1111/j.1525-1314.2010.00877.x

Exsolution of dolomite and application of calcite–dolomite solvus geothermometry in high-grade marbles: an example from Skallevikshalsen, East Antarctica

H. MIZUOCHI,[1] M. SATISH-KUMAR,[1] Y. MOTOYOSHI[2] AND K. MICHIBAYASHI[1]
[1]*Department of Geosciences, Shizuoka University, Ohya-836, Suruga-ku, Shizuoka 422-8529, Japan (smsatis@ipc.shizuoka.ac.jp)*
[2]*National Institute of Polar Research, 3-10 Midoricho, Tachikawa, Tokyo 190-8518, Japan*

ABSTRACT Calcite–dolomite solvus geothermometry is a versatile method for the estimation of metamorphic temperature because of its simplicity. However, in medium- to high-grade metamorphic rocks the accuracy of estimating temperature by the integration of unmixed dolomite and calcite is hampered by the heterogeneous distribution of unmixed dolomite, difficulties in distinguishing between preexisting and exsolved dolomite and demarcating grain boundaries. In this study, it is shown that calcite–dolomite solvus thermometry can be applied to calcite inclusions in forsterite and spinel for the estimation of peak metamorphic temperature in granulite facies marbles from Skallevikshalsen, East Antarctica. The marbles are comprised of a granoblastic mineral assemblage of calcite + dolomite + forsterite + diopside + spinel + phlogopite ± apatite, characteristic of granulite facies metamorphic conditions. Forsterite, spinel and apatite frequently contain 'negative crystal' inclusions of carbonates that display homogeneously distributed dolomite lamellae. On the basis of narrow ranges of temperature (850–870 °C) recorded from carbonate inclusions compared with the range from matrix carbonate it is regarded that the inclusion carbonates represent a closed system. Furthermore, this estimate is consistent with dolomite–graphite carbon isotope geothermometry, and is considered to be the best estimate of peak metamorphic temperature for this region. Matrix calcite records different stages of retrograde metamorphism and re-equilibration of calcite that continued until Mg diffusion ceased at ~460 °C. Electron backscattered diffraction (EBSD) results together with morphological features of unmixed coarse tabular dolomite suggest anisotropic diffusion and mineral growth are influenced by crystallographic orientation. Identification of sub-grain boundaries and formation of fine-grained unmixing in calcite rims suggest the presence of grain boundary fluids in the late retrograde stages of metamorphic evolution. These results, thus, demonstrate the usefulness of carbonate inclusion geothermometry in estimating the peak metamorphic temperatures of high-grade terranes and the application of EBSD in understanding the unmixing behaviour of minerals with solid solutions.

Key words: carbonate inclusion; electron backscattered diffraction; exsolution; marbles; solvus geothermometry.

INTRODUCTION

The estimation of peak metamorphic pressure and temperature (*P–T*) conditions of crustal rocks is important in understanding the thermal history, tectonic evolution and related metamorphic processes. High-grade metamorphic rocks, which form the dominant components of the lower crust, provide key information in deciphering the evolution of continental crust (e.g. Bohlen, 1987; Harley, 1989; Spear, 1993). Many existing thermobarometers yield a wide range of *P–T* conditions, depending on differing calibrations, and they therefore have limitations in their application to a particular system or bulk chemical composition. In addition, commonly used thermobarometers, in particular those based on cation exchange, usually yield lower *P–T* conditions than the peak, owing to extensive retrograde re-equilibration. Careful analyses and re-estimations are required to retrieve the peak *P–T* conditions (e.g. Fitzsimons & Harley, 1995; Pattison *et al.*, 2003). Calcite–dolomite solvus thermometry, a commonly used geothermometer for marbles, has similar drawbacks in this respect, although it has been successfully applied for marbles in the amphibolite facies conditions (Essene, 1982; Perkins *et al.*, 1982; Wada & Suzuki, 1983; Letargo *et al.*, 1995; Droop & Al-Filali, 1996; Dunn, 2005). However, in higher grades of metamorphism, the calcite–dolomite geothermometer has difficulties in its application because calcite can easily re-equilibrate by diffusion of Mg during retrograde metamorphism and form complex unmixing microstructures.

In a recent study, Müller *et al.* (2008) showed that crystal growth rate, diffusion and exsolution are important factors that affect the Mg distribution in calcite grains in contact aureoles. Although the distribution and morphology of the unmixed lamellae of dolomite are critical for the re-integration of Mg content in calcite for the estimation of temperature, studies focusing on the morphology of the unmixed lamellae are seldom undertaken. In mineral groups such as pyroxene and oxides, mineralogical studies have reported a crystallographic control on the orientation of unmixed lamellae in the host crystals. Exsolved phases are known to have orientation controls and a plane of best crystal structure fit with the host. Among early studies, Hess (1960) used the (010) *v.* (001) orientation of exsolved phases in ferromagnesian pyroxene to distinguish inverted pigeonite from original hypersthene. Buddington & Lindsley (1964) distinguished ilmenite in {111} planes of magnetite as of different origin than exsolution of spinel on {100} in magnetite. Furthermore, the orientation of exsolution was also used as a thermometer in augite (Jaffe *et al.*, 1975; Robinson *et al.*, 1977). Based on computational modelling using thermodynamic data under varying time-scales, Kuhl & Schmid (2007) suggested that the distribution pattern of exsolution in perthite or antiperthite follows the crystallographic orientation of the host crystal lattice. However, despite the preponderance of exsolution microstructures in the calcite–dolomite system and its wide application in thermometry, earlier studies have not attempted to evaluate the crystallographic control of dolomite exsolution. Recent advances in measuring the crystallographic orientation at the micrometre scale using electron backscattering diffraction (EBSD) technique has provided an opportunity to understand the crystallographic control of exsolution in further detail (e.g. Seto *et al.*, 2006).

A common means of understanding the *P–T–t–d* history of metamorphic rocks is to gather the information preserved in mineral inclusions in refractory minerals. This method has provided categorical evidence for ultra high pressure metamorphic conditions by the preservation of minerals such as coesite and diamond. Mineral inclusions have also been used in high-grade metamorphic rocks for understanding the metamorphic *P–T* evolution (Spear, 1993). However, marbles, a common lithological unit in high-grade terranes that contain granoblastic minerals such as forsterite, spinel and diopside, have rarely been examined from such a view point. Ferry (2001) suggested that calcite inclusions in forsterite may provide information on temperature of formation of the host minerals which would be less prone to retrograde alteration. Proyer *et al.* (2008) inferred the presence of former aragonite inclusions in marbles from the Greek Rhodope massif, and suggested that the marbles might have experienced ultra high pressure conditions, most likely at the aragonite–calcite transition. Thus, carbonate inclusions in high-grade metamorphic minerals are good candidates for extracting information on peak and prograde conditions in high-grade marbles.

In this study, calcite–dolomite solvus geothermometry was applied to estimate metamorphic temperature conditions using carbonate inclusions within forsterite, spinel and apatite in high-grade marbles from Skallevikshalsen, and to compare these temperatures with carbon isotope geothermometry. The successful application of carbonate inclusion thermometry suggests that it is a potential method for precise estimation of peak metamorphic temperatures in high-grade metamorphic terranes containing marbles. In addition, we attempt to understand the development of microstructures during unmixing of Mg–calcite formed at high temperature, based on the crystallographic relationships between host and unmixed lamellae using crystal preferred orientation data obtained by EBSD.

GEOLOGICAL BACKGROUND

General geology of the Lützow-Holm Complex

The Lützow-Holm Complex (LHC), one of several Pan-African metamorphic terranes that formed as a part of the East Gondwana supercontinent amalgamation, is located along the Prince Olav, Prince Herald and Soya coasts (~400 km), in East Antarctica (Fig. 1). A thick pile of metamorphosed pelitic and carbonate rocks is associated with granitic and mafic meta-igneous rocks, in a continental marginal tectonic setting and oceanic closure during the Gondwana amalgamation (Satish-Kumar *et al.*, 2008a). Based on a detailed chemostratigraphic investigation using carbon, oxygen and strontium isotope systematics, Satish-Kumar *et al.* (2008b) ascribed a Neoproterozoic age (*c.* 830–730 Ma) of deposition for carbonate rocks in this region. These sedimentary rocks experienced a progressive metamorphism from amphibolite facies at the Prince Olav coast to granulite facies at the Soya coast (Shiraishi *et al.*, 1989; Hiroi *et al.*, 1991), and attained ultra high temperature conditions at Rundvågshetta (Motoyoshi & Ishikawa, 1997). The thermal maximum and the deepest crustal levels are located at the Lützow-Holm bay, around Rundvågshetta, perhaps indicating that the LHC is possibly an oblique crustal section formed during the final amalgamation of East Gondwana (Jacobs & Thomas, 2004; Satish-Kumar *et al.*, 2008a). Based on petrological studies on a suite of metamorphic rocks from Rundvågshetta, Motoyoshi & Ishikawa (1997) estimated peak metamorphic conditions of ~1000 °C and 11 kbar. The presence of kyanite and staurolite inclusions within garnet porphyroblasts and plagioclase along with decompression corona textures suggests that the LHC experienced a 'clockwise' *P–T–t* path (Motoyoshi *et al.*, 1989; Hiroi *et al.*, 1991). The age of peak

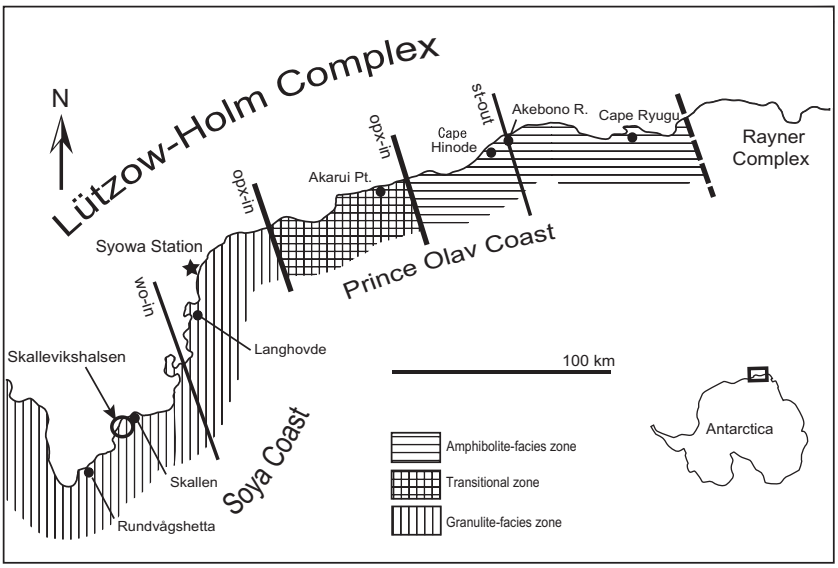

Fig. 1. Simplified geological map of the Lützow-Holm Bay region. Progressive increase in metamorphic grade along the Prince Olav Coast to the Soya Coast is based on Shiraishi *et al*. (1989). Bold lines show the isograds identified by Hiroi *et al*. (1991).

metamorphism in the LHC is between 553 ± 6 and 521 ± 9 Ma, as inferred from SHRIMP U–Pb zircon data (Shiraishi *et al*., 1994, 2008); however, new data on monazite CHIME geochronology also indicate an older population of ages *c*. 600 Ma (Hokada & Motoyoshi, 2006). Using U–Pb, K/Ar and Ar/Ar ages, Fraser *et al*. (2000) suggested that the evolution and preservation of symplectic coronas surrounding peak mineral assemblages are indicative of a rapid exhumation (3 km Myr^{-1}) and cooling (30 °C Myr^{-1}) of the lower crust during retrograde metamorphism.

Geology of Skallevikshalsen

Rock types, structure and metamorphism

Skallevikshalsen is located in the Lützow-Holm Bay coast, ~70 km southwest of Syowa Base (Fig. 1). The basement rocks in this region comprise a variety of meta-sedimentary and meta-igneous rocks including orthogneiss (pyroxene gneiss, granitic gneiss and metabasite), paragneiss, marble and skarn (Fig. 2; Yoshida *et al*., 1976). Pyroxene gneisses are the most widely distributed rock type, which are intruded by a number of granitic pegmatites (Yoshida *et al*., 1976). Skarn occurs at the contact between marble and leucogneisses. Metabasites occur as lenses and layers within orthogneiss and paragneiss. Two thick marble layers in the region commonly contain enclaves of adjacent lithologies. All the lithological units have NE–SW strike with a gentle dip towards SE (< 40 °). These lithologies, except for the granitic pegmatites, experienced strong deformation. Kawakami & Ikeda (2004) identified four deformational events during retrograde metamorphism in this region, namely D_{m-2}, D_{m-1}, D_m, D_{m+1}, represented by sillimanite alignment in garnet rims, rootless isoclinal folds, tight folds and open folds, respectively. Metamorphic *P–T* conditions of Skallevikshalsen, using conventional cation exchange thermobarometry and net-transfer equilibria in mafic gneiss are estimated at ~780–960 °C and 6–11 kbar (Yoshimura *et al*., 2004).

Field relations and sample descriptions

Field studies and sampling in Skallevikshalsen were carried out during the 46th Japanese Antarctic Research Expedition (2004–2005). About 50 marble samples were collected from the two main marble layers, one in the north side of the outcrop and the other in the south (Fig. 2). The northern marble layer is massive, has a gentle dip towards the SE and is overlain by pyroxene gneiss and underlain by granitic gneiss. The southern marble layer shows strong gneissose banding with rhythmic alternation of silicate-rich layers and pure dolomite layers (Fig. 3a). Both the layers enclose decimetre-sized mica-rich boudins.

Thin section petrography and staining of marble slabs with Alizarin Red-S were carried out on all samples (Fig. 3b). The staining method follows the procedure recommended in Dickson (1965). Calcite is stained to a pink to red colour, whereas dolomite or other silicate minerals are not stained. Calcite and dolomite together composes > 90% of the marbles, except in the silicate-rich layers. The marbles exhibit a granoblastic texture with medium to coarse grain size (~1–10 mm). In layers that contain abundant silicate minerals, calcite is the dominant carbonate. However, dolomite is predominant in layers in which silicate minerals are scarce.

ANALYTICAL METHODS

The distribution and textural relations of major minerals in the marble, especially the carbonates, were examined using cathodoluminescence (Premier

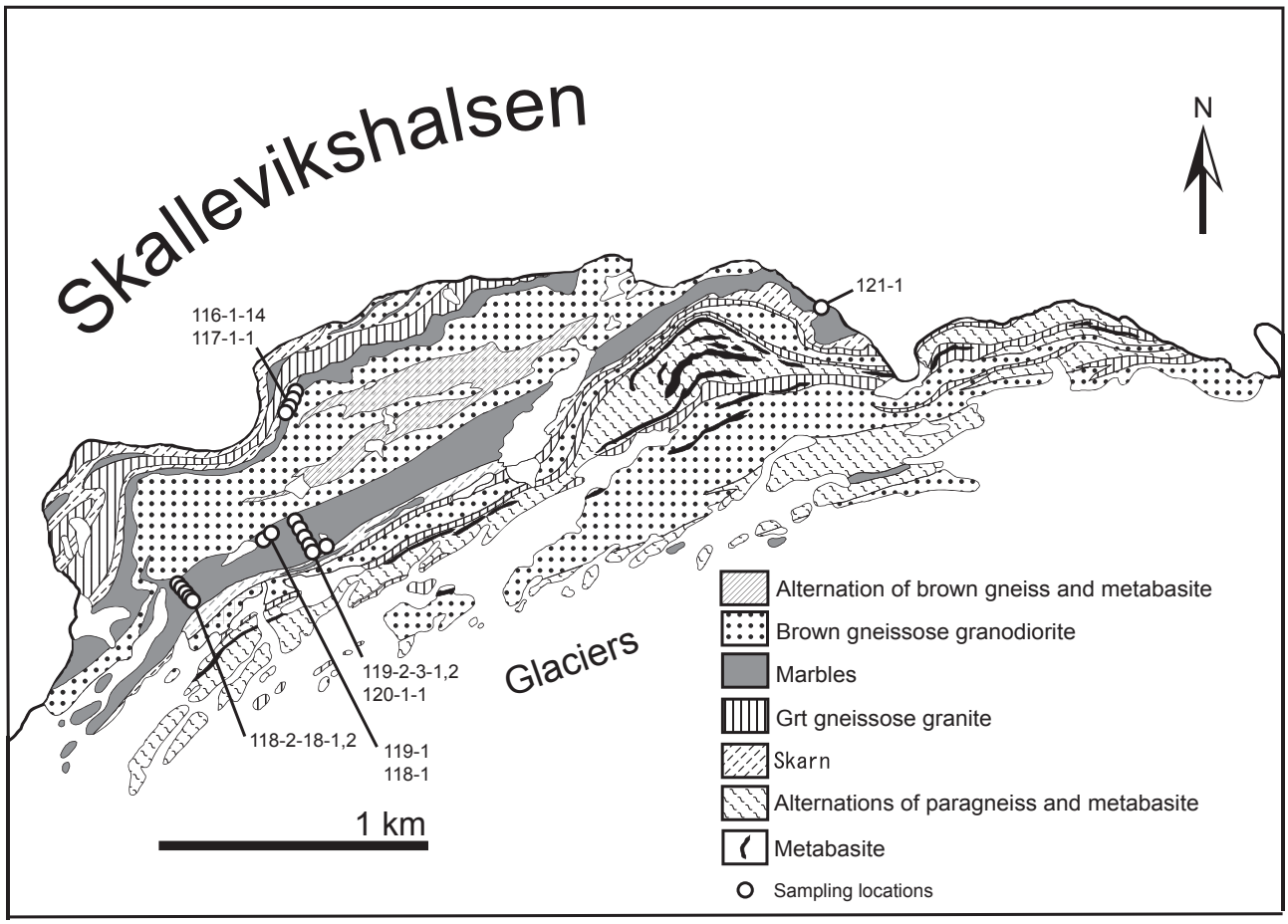

Fig. 2. Geological map of Skallevikshalsen region in the Lützow-Holm Complex (Yoshida *et al.*, 1976), showing sampling locations in this study.

American Technologies Luminoscope ELM-3R at Shizuoka University) under analytical conditions described in Satish-Kumar *et al.* (2006b). In general, calcite shows red luminescence, whereas dolomite is relatively dark red. Retrograde diopside formed after forsterite shows yellowish-green luminescence and forsterite does not show any luminescence.

The measurement of mineral compositions and backscattered electron imaging (BSE) were carried out on selected samples using a JEOL JCXA-733 electron microprobe (EMP) at the Centre for Instrumental Analysis, Shizuoka University. Analytical conditions were 12 nA beam current, 15 kV accelerating voltage and a minimum beam diameter of 1–3 μm for silicate minerals. A defocused beam of $\sim$10 μm was used for carbonate minerals. Carbonates containing exsolution lamellae smaller than 10 μm were measured using a broad beam of diameter 50 μm to obtain an average chemical composition. The chemical compositions of phlogopite and pargasite, including F and Cl, were analysed using the JEOL JXA-8621 EMP at Tsukuba University. Analytical conditions were 40 nA beam current and 15 kV accelerating voltage with a beam diameter of 20 μm. The Bence & Albee (1968) correction with modified α parameters of Nakamura & Kushiro (1970) was used for the EMP data at Shizuoka University, whereas an oxide-ZAF correction was applied for the EMP results at Tsukuba University. Compositional mapping of selected areas of matrix calcite showing exsolution textures were obtained using a JEOL JXA-8800M EMP at the National Institute of Polar Research, Tokyo.

Crystallographic preferred orientations (CPO) of carbonate minerals were measured by indexation of EBSD patterns using a JEOL JSM-6300 system at the Centre for Instrumental Analysis, Shizuoka University, operated at an accelerating voltage of 20 kV and beam current of 6 nA. EBSD patterns were indexed using CHANNEL+ software from HKL technology (Schmidt & Olesen, 1989).

Stable isotope compositions of carbon and oxygen in carbonate minerals and carbon in graphite were measured using a Finnigan MAT 250 Mass Spectrometer at Shizuoka University. Calcite and dolomite samples were scraped using a knife edge from a polished and stained marble slab. The powder was then

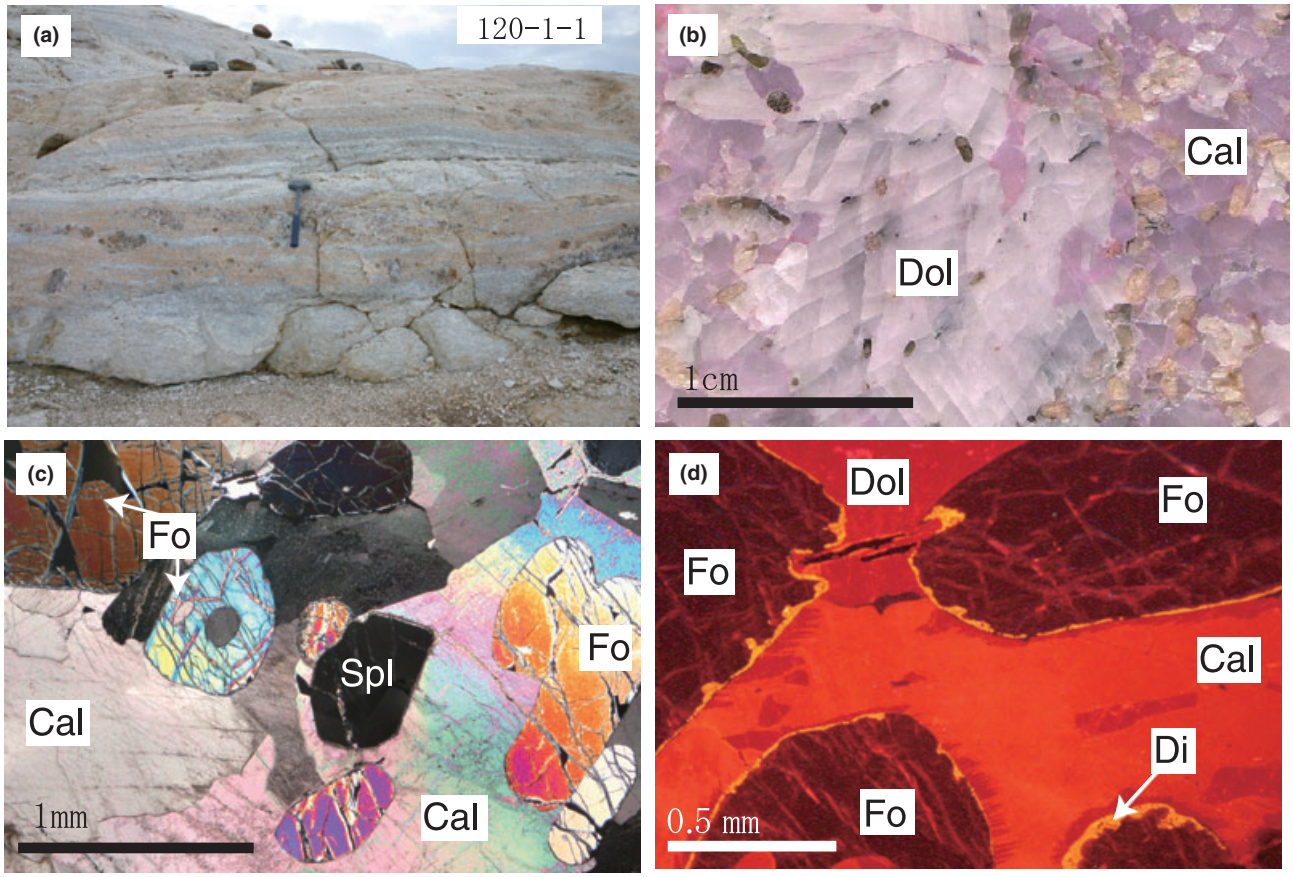

Fig. 3. (a) Field photograph of the marble outcrop at Skallevikshalsen, showing alternating dolomitic marble and silicate-rich marble layers. The marble samples from the southern marble layer (location ST050120-1) including mica-rich blocks was collected from this outcrop. (b) Photographs of marble slab stained with Alizarin Red-S. Calcite in silicate-rich layer is stained pink to red colour and dolomite-rich band is not stained (scale bar = 1 cm). (c) Photomicrograph of marble sample showing the common mineral assemblages (crossed polar, scale bar = 1 mm). Note that forsterite contains carbonate inclusions. (d) Cathodoluminescence image of carbonate and silicate minerals showing thin rims of diopside and dolomite surrounding forsterite, and exsolution lamellae of dolomite within matrix calcite (scale bar = 0.5 mm).

placed in a small stainless steel cup and dropped into a vessel containing phosphoric acid at 60 °C under vacuum to produce CO_2 (Wada *et al.*, 1984a). The carbonate reaction system is connected with an online gas purification system of pentane slush to remove H_2O, and transported to the inlet system of the mass spectrometer. The results are reported in conventional δ notation relative to the V-PDB (Vienna Belemnitella Americana from Peedee Formation) standard for carbon and the V-SMOW (Vienna Standard Mean Ocean Water) standard for oxygen. Graphite was separated directly from the marble slabs, cleaned with 2N HCl, and placed in Vycor tubes (6φ), together with excess of V_2O_5 as oxidizing agent. Beforehand, the Vycor tubes were heated at 1000 °C for 10 h to remove contaminants (Wada *et al.*, 1984b). The Vycor tubes containing graphite and V_2O_5 were again preheated to remove contaminants in samples at 500 °C for 30 min, and sealed under vacuum ($\sim 10^{-3}$ Torr). Sealed tubes were then combusted at 1000 °C for 2 h to oxidize graphite to CO_2. The sealed tubes were then cracked and open to the inlet system to extract the CO_2 for measuring the carbon isotopes.

PETROGRAPHY OF MARBLES

The marbles are medium- to coarse-grained with well-annealed granoblastic polygonal textures (Fig. 3c). Carbonate grains have an average diameter in the range of 1–10 mm, generally larger than the associated silicate minerals. The marbles are characterized by an equilibrium peak metamorphic mineral assemblage of calcite + dolomite + forsterite + diopside (Table 1). Additionally, phlogopite, pargasite, apatite, spinel, rutile and graphite are observed in some layers in varying proportions. Forsterite tends to form subequant to rounded grains. Diopside is anhedral, whereas spinel, pargasite and apatite are subhedral to euhedral. Phlogopite has a tendency to form aggregates of large crystals (up to few mm).

Table 1. Mineral assemblages of marbles from Skallevikshalsen, Lützow-Holm Complex. Abbreviations from Kretz (1983).

Sample no.	Mineral assemblage
116-1-14	Cal + Dol + Fo + Di + Spl + Phl + Prg ± Rt ± Gr
117-1-1	Cal + Dol + Fo + Di + Spl + Phl + Prg
118-2-18	Cal + Dol + Fo + Di + Spl + Phl + Prg + Ap + Gr
119-2-3-1,2	Cal + Dol + Fo + Di + Spl + Phl + Gr
120-1-1	Cal + Dol + Fo + Di + Spl + Phl + Gr
121-1	Cal + Dol + Fo + Di + Spl + Phl ± Rt ± Gr

Forsterite + spinel + diopside assemblage is interpreted to be in equilibrium, which is characteristic of granulite facies metamorphic condition (Ferry, 2001; Satish-Kumar *et al.*, 2001). Thin reaction rims of dolomite and diopside surround forsterite (Fig. 3d), indicating that it was partially replaced by dolomite and diopside during retrograde metamorphism, which in turn suggests that forsterite was a stable phase during peak metamorphism. The forsterite shows fine veins of serpentine (Fig. 3c,d), indicating hydration reactions in the late stage of retrograde metamorphism.

Morphology of exsolved dolomite

Morphological characterization of unmixed dolomite from calcite was carried out using petrography, BSE image analysis and elemental mapping in multiple grains within single thin sections as well as in different samples from several localities at Skallevikshalsen. First, the size distribution varies markedly in different unmixed zones within single grains (Fig. 4). The core portions of the calcite grains often display coarse dolomite lamellae ranging up to hundreds of micrometres in length, which are surrounded by zones with fine-grained exsolution (Fig. 4c). Second, there is noticeable difference in the shape of unmixed dolomite

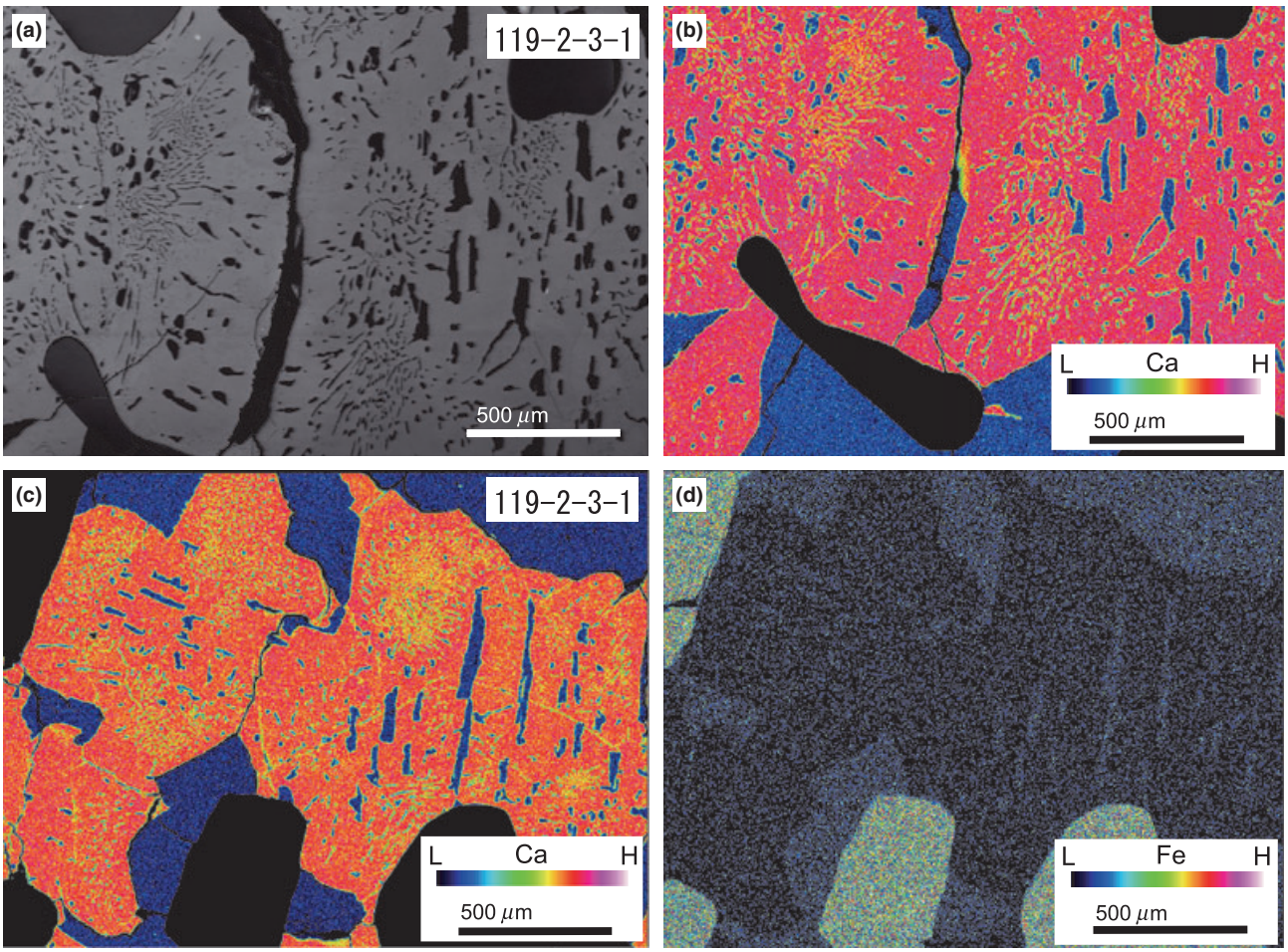

Fig. 4. Photomicrograph of: (a) backscattered electron image and (b) compositional image of same area as in (a) showing heterogeneity in the distribution of dolomite lamellae, while the compositions are homogeneous for dolomite and calcite. (c) Calcium distribution map of unmixed calcite grains showing different sizes, shapes and distribution of dolomite lamellae. (d) Distribution of Fe in calcite dolomite and forsterite. H and L represent higher and lower X-ray intensity, which reflects higher and lower concentrations of Ca, respectively.

in the two different zones described before, the former coarse unmixed dolomite is characterized by tabular elongated shape with aspect ratios as high as 1:12 (width:length). In contrast, the fine-grained unmixed dolomite comprises of wormy or elliptical or spherical blebs with lower aspect ratios. To observe the three-dimensional shapes of exsolved dolomite, slabs of marbles complimentary to the thin sections were etched with 2N HCl and observed under reflected light optical microscope. The coarse exsolved dolomite were confirmed to be of tabular in shape, whereas the fine-grained exsolution formed irregular blebs, as described in Kretz (1988) and Ogasawara *et al*. (1998).

Carbonate inclusions in forsterite, spinel and apatite

Carbonate inclusions can be considered as a closed system after the time of entrapment and may preserve information about the prograde to peak metamorphic conditions. As described in Ferry (2001), inclusions have to be carefully selected from the standpoint of size, shape and relation to its host grain to avoid changes in their chemical composition during retrograde metamorphism. Forsterite, spinel and apatite in marbles at Skallevikshalsen contain well-preserved carbonate mineral inclusions. Care was taken to avoid inclusions which are located in the edge of the host crystal or those cut across by serpentine veins. In addition, cathodoluminescence microscopy was employed to avoid inclusions associated with retrograde minerals surrounding the inclusions. Inclusions having a diameter >100 μm were selected. Most calcite inclusions in forsterite are oval in shape (Fig. 5a); in spinel, some are nearly octagonal; and in apatite, they are hexagonal (Fig. 5f). These inclusions, likely exhibit 'negative crystal' shapes suggesting their capture during the formation of the host mineral. Based on the textures and distribution of calcite and dolomite within the inclusions, three types were distinguished.

Type 1 inclusions consist of well-defined coarse crystals of calcite and dolomite (Fig. 5a). They are usually found in forsterite, oval in shape and have a diameter of up to 500 μm. The boundary between calcite and dolomite is variable, from straight to irregular indicating large variations in shape of the dolomite within the inclusion.

Type 2 inclusions are characterized by relatively homogeneous exsolution textures (Fig. 5b,c,f). They occur as oval to spherical shapes in forsterite and are faceted in spinel and apatite, showing 'negative crystal' shapes. Type 2 inclusions are generally smaller in size than Type 1 inclusions. However, inclusions >100 μm are common. The peculiarity of the Type 2 inclusions is that they show homogenous dolomite unmixing, except along the rim of the inclusion, where grain coarsening is observed (Fig. 5b,c). The unmixed dolomite grains within the inclusions in forsterite are commonly elliptical to spherical in shape, whereas those in apatite have a wormy texture (Fig. 5f).

Type 3 inclusions are more or less monomineralic (Fig. 5d). These inclusions are mostly found in forsterite and have diameter >200 μm. Both calcite and dolomite inclusions are observed. Calcite inclusions occasionally contain micrometre-size lamellae of dolomite.

In addition to the aforementioned types, composite types of inclusions also occur, which display a combination of exsolution textures (Fig. 5e). Inclusions with irregular shapes were also observed in forsterite, which were not considered in this study.

MINERAL CHEMISTRY

The calcite in the marbles is magnesian (Table 2). There is no compositional difference between calcite in the matrix and inclusions (Fig. 6). Matrix calcite in marbles has low Mg contents (X_{Mg}), mostly 0.06 ± 0.01 a.p.f.u (average of 50 analyses). However, a few measurements gave Mg contents up to 0.10 a.p.f.u. The electron beam might have stepped over to a nearby dolomite crystal or the measurement spot might have contained micrometre-scale exsolution lamellae, similar to those observed in Müller *et al.* (2008). Most matrix dolomite has Mg contents in the range of 0.44–0.49 a.p.f.u., and the lowest measured value is $\sim$0.39 a.p.f.u. Although Fe contents are negligible in calcite and dolomite, dolomite has slightly higher Fe content than calcite (Fig. 6 & Table 2). Furthermore, the composition of exsolved dolomite in matrix calcite is similar to that of matrix dolomite, whereas calcite within the inclusions has a larger range of Fe contents (0.003–0.010 a.p.f.u.), irrespective of the types. The X_{Mg} values of calcite in inclusions vary widely between 0.049 and 0.079, although Type 2 inclusions have a narrow range (0.049–0.068). In contrast, X_{Mg} values of unmixed dolomite within the inclusions does not vary much (0.460–0.482).

Forsterite and spinel are very close to the Mg end-member composition (Table 3), and clinopyroxene in marbles is very close to diopside in composition, irrespective of textural settings. Secondary diopside, formed as reaction rims surrounding forsterite, has a similar composition to that of primary diopside. Phlogopite in marbles has average fluorine contents ranging from 0.40 to 0.66 a.p.f.u., and has average Mg number of 97–99. Amphibole is close to pargasite end-member, and has a fluorine content ranging from 0.15 to 0.45 a.p.f.u. (Table 4).

MINERAL REACTION HISTORY

The prograde reaction history of the high-grade marbles at Skallevikshallsen is difficult to infer because of the absence of low-grade equivalents in the LHC. The equilibrium granoblastic mineral assemblages of the marble samples were products of prograde reactions in an impure dolomitic limestone with varying proportions of quartz, feldspar and clay minerals as detrital

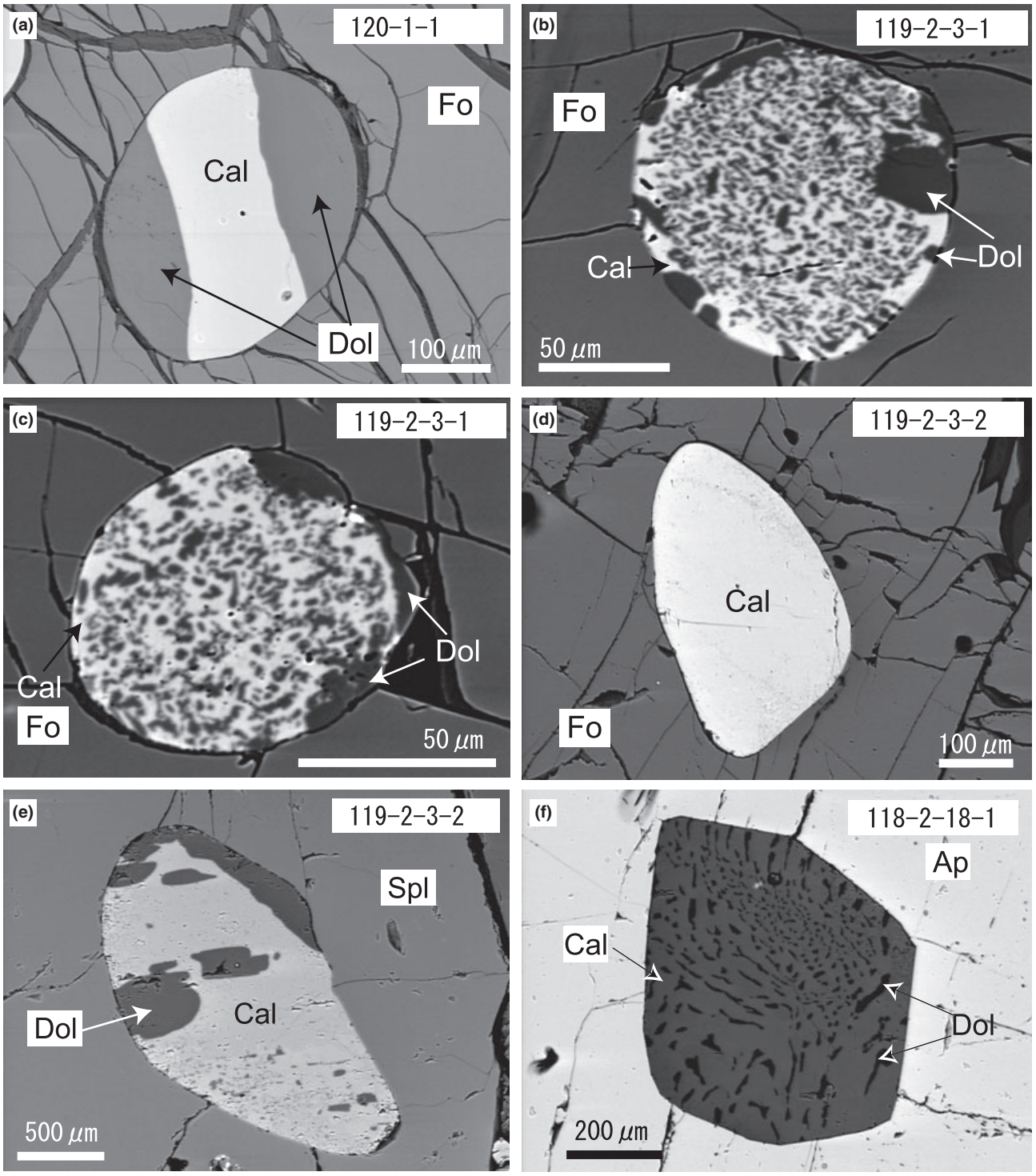

Fig. 5. Backscattered electron images show various shapes of carbonate inclusions. (a) Type 1 inclusions with sharp boundary between calcite and unmixed dolomite. Carbonate inclusions in spinel are most frequently circular or elliptical in shape. (b,c) Type 2 spherical or elliptical carbonate inclusions with negative crystal shapes are observed in forsterite. Note that the rims of the inclusions show coarsening of dolomite. (d) A Type 3 calcite inclusion in forsterite. (e) A composite inclusion in spinel showing heterogeneous unmixing of dolomite in calcite. (f) A faceted negative crystal inclusion in apatite with wormy exsolution lamellae.

components. As a result of the high-T metamorphism none of these detrital components remain, not even the remnants of early prograde minerals could be found as inclusions. However, because of the simple chemical composition of the minerals, it is possible to model the prograde to peak metamorphic mineral reactions in the

Table 2. Representative electron microprobe analytical results of calcite and dolomite.

Calcite										
Textural site	Matrix			Inclusion (forsterite)				Inclusion (spinel)		Inclusion (apatite)
Sample no.	120-1-1(2)	120-1-1(6)	120-1-1(8)	116-1-14	118-2-18	119-2-3	120-1-1(8)	116-1-14	119-2-3	118-2-18
FeO	0.25	0.25	0.28	0.22	0.26	0.35	0.27	0.10	0.26	0.24
MnO	0.16	0.18	0.16	0.14	0.19	0.22	0.17	0.17	0.19	0.17
MgO	3.17	3.18	3.19	2.00	2.67	2.75	2.73	2.05	2.60	1.87
CaO	52.61	52.05	52.11	54.53	52.80	52.14	52.51	54.44	53.13	54.44
Total	56.37	55.81	55.92	56.89	55.92	55.46	55.69	56.75	56.18	56.72
Formula	1(O)									
Fe	0.003	0.003	0.004	0.003	0.004	0.005	0.004	0.001	0.004	0.004
Mn	0.002	0.002	0.002	0.002	0.003	0.003	0.002	0.002	0.003	0.003
Mg	0.077	0.078	0.078	0.048	0.065	0.068	0.067	0.050	0.063	0.063
Ca	0.914	0.913	0.912	0.944	0.925	0.921	0.924	0.945	0.928	0.928
Total	1.004	1.003	1.004	0.997	0.997	0.996	0.997	0.998	0.997	0.997

Dolomite												
Textural site	Matrix			Matrix (exsolution)		Inclusion (forsterite; exsolution)				Inclusion (spinel; exsolution)		Inclusion (apatite)
Sample no.	120-1-1(2)	120-1-1(6)	120-1-1(8)	120-1-1(6)	120-1-1(8)	116-1-14	118-2-18	119-2-3	120-1-1(8)	116-1-14	119-2-3	118-2-18
FeO	0.42	0.39	0.36	0.43	0.42	0.30	0.45	0.75	0.44	0.25	0.58	0.59
MnO	0.15	0.16	0.16	0.13	0.13	0.24	0.15	0.19	0.17	0.14	0.17	0.18
MgO	21.00	21.21	20.25	20.78	21.20	16.01	20.68	19.30	20.62	20.27	19.49	20.77
CaO	30.93	30.86	29.36	31.01	31.09	36.61	31.14	31.44	31.43	30.93	30.94	31.50
Total	52.67	52.76	50.28	52.50	52.99	53.16	52.41	51.67	52.66	51.59	51.18	53.03
Formula	1(O)											
Fe	0.005	0.005	0.005	0.006	0.005	0.004	0.006	0.010	0.006	0.003	0.008	0.007
Mn	0.002	0.002	0.002	0.002	0.002	0.003	0.002	0.003	0.002	0.002	0.002	0.002
Mg	0.481	0.484	0.485	0.477	0.482	0.375	0.475	0.454	0.472	0.473	0.461	0.472
Ca	0.509	0.506	0.505	0.512	0.508	0.616	0.514	0.531	0.517	0.519	0.526	0.515
Total	1.003	1.003	1.003	1.003	1.003	0.997	0.997	0.997	0.997	0.997	0.997	0.997

$CaO–MgO–Al_2O_3–SiO_2–H_2O–CO_2$ system (CMASHC; Fig. 7). The $T–X_{CO2}$ reaction grid was constructed using THERMOCALC (Powell & Holland, 2001). A total pressure of 10 kbar was assumed as the peak metamorphic pressure condition (estimated by Yoshimura *et al.*, 2004). The diagram shows that the reaction that produced tremolite occurred in the earlier stages of the prograde metamorphism. Forsterite and phlogopite formed with progress of the prograde reactions during increasing temperature and X_{CO2}. Although forsterite in marbles appears at a variety of temperatures, regardless of the composition of the fluid, based on petrography the following reaction is considered to be the most probable one during prograde (near the peak) metamorphism:

$$4\,\text{dolomite} + \text{diopside} = 4\,\text{calcite} + 2\,\text{forsterite} + 2CO_2.$$

The marbles also display retrograde reaction textures that overprint the peak metamorphic assemblages, which can be clearly distinguished in the cathodoluminescence images (Fig. 3d). Forsterite grains are surrounded by thin rims of dolomite and diopside produced by earlier stage retrograde reaction.

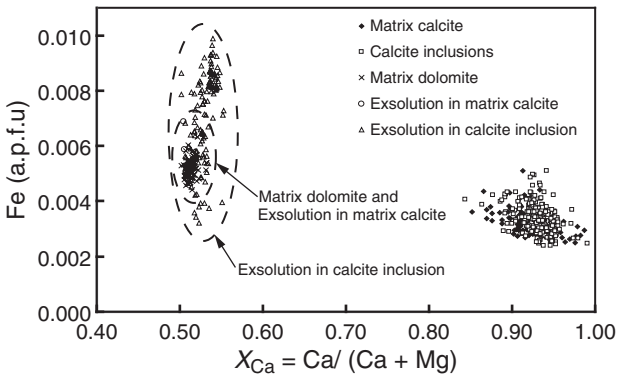

Fig. 6. Chemical compositional variation of X_{Ca} and Fe of carbonate minerals and inclusions from marbles were observed. Calcite and dolomite compositions were normalized to one cation.

GEOTHERMOMETRY

Calcite–dolomite solvus geothermometry

The calcite + dolomite geothermometer has been well characterized both experimentally and thermodynamically (e.g. Goldsmith & Newton, 1969; Powell *et al.*, 1984; Anovitz & Essene, 1987). These formulations have been used to constrain the metamorphic temperatures in many amphibolite facies metamorphic terranes (Perkins *et al.*, 1982; Letargo *et al.*, 1995; Droop & Al-Filali, 1996; Dunn, 2005). Equilibrium temperatures can be estimated from compositions of coexisting calcite + dolomite miscibility gap or solvus (Anovitz & Essene, 1987). However, owing to

Table 3. Representative electron microprobe analytical results of forsterite, diopside and spinel.

Mineral	Forsterite					Diopside			Spinel			Rutile
Sample no.	116-1-13	116-1-14	116-1-16	117-1-1	120-1-1	116-1-14	116-1-16	120-1-1	116-1-16	117-1-1	120-1-1	116-1-16
SiO_2	42.34	41.28	41.33	41.57	42.15	54.04	52.82	55.10	0.12	0.13	0.15	0.17
TiO_2	0.23	0.00	0.00	0.00	0.00	0.00	0.00	0.00	0.23	0.26	0.24	99.20
Al_2O_3	0.09	0.00	0.00	0.00	0.00	0.59	1.24	0.59	69.38	67.15	70.11	0.14
FeO	1.09	1.14	1.61	1.29	1.87	0.29	0.46	0.41	1.92	1.16	1.96	0.40
MnO	0.15	0.14	0.16	0.18	0.14	0.16	0.15	0.14	0.15	0.16	0.13	0.16
MgO	55.84	57.99	55.66	57.53	54.73	19.05	18.83	18.47	26.38	25.12	26.67	0.00
CaO	0.13	0.00	0.00	0.00	0.00	25.50	25.27	25.57	0.11	0.13	0.12	0.14
Na_2O	0.05	0.00	0.00	0.00	0.00	0.00	0.00	0.00	0.06	0.13	0.07	0.11
K_2O	0.09	0.00	0.00	0.00	0.00	0.00	0.00	0.00	0.08	0.09	0.08	0.10
V_2O_3	0.25	0.00	0.00	0.00	0.00	0.00	0.00	0.00	0.39	0.32	0.29	0.00
Cr_2O_3	0.11	0.00	0.00	0.00	0.00	0.00	0.00	0.00	0.21	0.12	0.12	0.00
NiO	0.19	0.00	0.00	0.00	0.00	0.00	0.00	0.00	0.20	0.25	0.16	0.31
Total	100.56	100.56	98.77	100.56	98.89	99.62	98.78	100.28	99.24	95.00	100.09	100.72
Formula	4 (O)					6 (O)			4 (O)			2 (O)
Si	0.99	0.97	0.99	0.98	1.01	1.96	1.94	1.98	0.00	0.00	0.00	0.00
Ti	0.00	0.00	0.00	0.00	0.00	0.00	0.00	0.00	0.00	0.00	0.00	0.99
Al_{total}	0.00	0.00	0.00	0.00	0.00	0.03	0.05	0.03	1.98	1.99	1.98	0.00
Fe	0.02	0.02	0.03	0.03	0.04	0.01	0.01	0.01	0.04	0.02	0.04	0.00
Mn	0.00	0.00	0.00	0.00	0.00	0.00	0.00	0.00	0.00	0.00	0.00	0.00
Mg	1.96	2.03	1.99	2.02	1.95	1.03	1.03	0.99	0.95	0.94	0.95	0.00
Ca	0.00	0.00	0.00	0.00	0.00	0.99	0.99	0.99	0.00	0.00	0.00	0.00
Na	0.00	0.00	0.00	0.00	0.00	0.00	0.00	0.00	0.00	0.01	0.00	0.00
K	0.00	0.00	0.00	0.00	0.00	0.00	0.00	0.00	0.00	0.00	0.00	0.00
V	0.00	0.00	0.00	0.00	0.00	0.00	0.00	0.00	0.01	0.01	0.01	0.00
Cr	0.00	0.00	0.00	0.00	0.00	0.00	0.00	0.00	0.00	0.00	0.00	0.00
Ni	0.00	0.00	0.00	0.00	0.00	0.00	0.00	0.00	0.00	0.01	0.00	0.00
Total	3.00	3.03	3.01	3.02	2.99	4.02	4.03	4.00	3.00	3.00	3.00	1.01

Table 4. Representative electron-microprobe analytical results of phlogopite and amphibole.

Mineral	Phlogopite		Amphibole		
Sample no.	116-1-15	120-1-1	116-1-15	116-1-16	117-1-1
SiO_2	41.67	39.22	45.61	43.88	44.94
Al_2O_3	15.38	17.18	14.30	15.34	14.09
TiO_2	1.39	1.59	1.48	4.11	0.32
Cr_2O_3	0.03	0.00	0.07	0.04	0.01
FeO	0.48	0.45	0.59	0.55	0.24
MnO	0.00	0.02	0.00	0.00	0.02
MgO	27.20	25.80	20.74	19.92	19.87
CaO	0.07	0.00	13.06	13.15	12.63
Na_2O	0.84	0.64	3.07	2.95	2.79
K_2O	11.21	10.74	0.84	0.29	0.56
ZnO	0.00	0.00	0.02	0.00	0.03
F	1.33	1.23	0.56	0.35	0.88
O	−0.56	−0.52	−0.24	−0.15	−0.37
Cl	0.11	0.06	0.16	0.16	0.18
O	−0.02	−0.01	−0.04	−0.04	−0.04
H_2O	4.19	4.12	1.98	2.09	1.74
Total	103.31	100.52	102.20	102.63	97.90
Formula	22 (O)		23 (O)		
Si	5.09	4.92	5.95	5.71	6.06
Al	2.22	2.54	2.20	2.35	2.24
Ti	0.13	0.15	0.15	0.40	0.03
Cr	0.00	0.00	0.01	0.00	0.00
Fe	0.05	0.05	0.06	0.06	0.03
Mn	0.00	0.00	0.00	0.00	0.00
Mg	4.96	4.83	4.03	3.86	3.99
Ca	0.01	0.00	1.82	1.83	1.82
Na	0.20	0.16	0.78	0.75	0.73
K	1.75	1.72	0.14	0.05	0.10
Zn	0.00	0.00	0.00	0.00	0.00
F	0.51	0.49	0.23	0.14	0.38
Cl	0.02	0.01	0.04	0.04	0.04
H_2O	3.42	3.45	1.72	1.81	1.56
Total	18.35	18.32	17.13	17.01	16.99

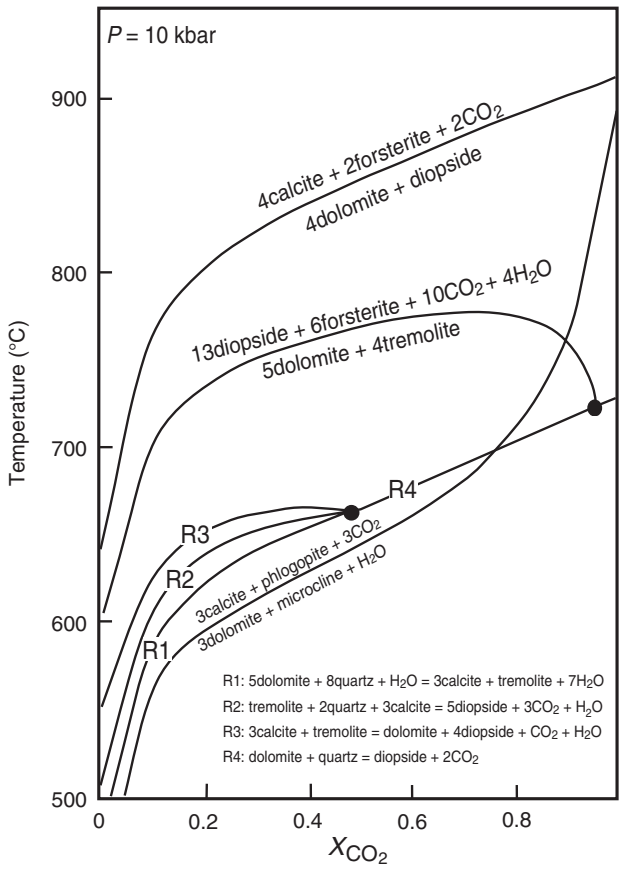

Fig. 7. *T–X* diagram at 10 kbar for the system K_2O–CaO–MgO–Al_2O_3–SiO_2–H_2O–CO_2. The stability of the phases was calculated using THERMOCALC.

retrograde re-equilibration of Ca and Mg between calcite and dolomite, the calcite + dolomite solvus geothermometer is not considered suitable for high-grade rocks. Generally, reintegration methods between calcite and dolomite exsolution are applied to determine peak metamorphic temperatures, whereas re-equilibrated magnesian calcite compositions might give some information on closure of diffusion (e.g. Letargo *et al*., 1995; Piazolo & Markl, 1999).

Temperature estimates for matrix calcite

Calcite–dolomite solvus geothermometry was applied using the formulation (23) of Anovitz & Essene (1987) as given in the following:

$$T_{(\mathrm{K})} = A(X_{\mathrm{Mg}}) + B/(X_{\mathrm{Mg}})^2 + C(X_{\mathrm{Mg}})^2 + D(X_{\mathrm{Mg}})^{0.5} + E,$$

where A, B, C, D and E are coefficients with values −2360.0, −0.01345, 2620.0, 2608.0 and 334.0, respectively, and X_{Mg} is the Mg content [Mg/(Ca + Mg) a.p.f.u.] of calcite. Although this formulation does not account for Fe in the system, it is still suitable for this study because Fe was barely detected in the carbonates (Table 2). Analyses of 38 grains of the non-reintegrated matrix calcite gave temperatures of 460–720 °C (Fig. 8). Based on experimental diffusion coefficients, Fisler & Cygan (1998) suggested that in regional metamorphic terranes, where cooling rates are in the order of 1 °C Myr^{-1} compositions in calcite will be reset above 500 °C for normally observed grain size. The lowest temperature estimates recorded in calcite in our study is consistent with this model, and possibly indicates the closure temperature of Mg diffusion and unmixing during cooling. However, temperatures estimated for matrix calcite grains, reintegrating selected domains comprising homogeneously exsolved dolomite lamellae, lie in the range between 720 and 760 °C. Reintegration was carried out by estimating the composition prior to unmixing, from the present compositional data and estimating the area of calcite and dolomite using a digital BSE image and the image analysis software 'Scion Image^{TM}'. Broad beam analysis technique was also employed where exsolution lamellae were smaller than the electron beam diameter of 10 μm. As expected, this estimate is considerably lower than the peak metamorphic temperature estimates in metapelitic rocks from the same region (Yoshimura *et al*., 2004). The causes for such lower temperature estimates might be owing to the heterogeneous distribution of the exsolved phases and possible presence of preexisting carbonates (Fig. 4a,b). Moreover, dolomite and/or calcite can also be a product phase of retrograde reaction, which is difficult to distinguish between the exsolved and preexisting grains.

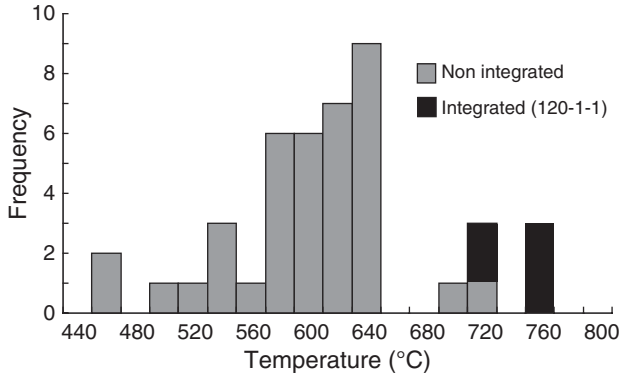

Fig. 8. Frequency distribution diagram of non-integrated temperatures inferred from the composition of analysed matrix calcite in 38 grains. The histograms exhibit a near Gaussian shape. These temperatures range from 460 to 720 °C. Temperatures estimated for five grains showing homogenous exsolution textures are also shown.

Temperature estimates for calcite inclusions

In this study, 14 inclusions from forsterite, spinel and apatite were analysed in detail. The chemical composition of the calcite and dolomite lamellae within the inclusions were reintegrated using BSE images and the image analysis software 'Scion Image^{TM}'. The results gave a wide spectrum of temperatures from ~600 °C to in excess of 1000 °C (Table 5). The estimated temperatures for Type 1 inclusions (three grains) are between 970 and 1020 °C. The temperature estimates for Type 2 inclusions (four grains) in forsterite are between 850 and 860 °C; those within spinel yield 850–870 °C and one Type 2 inclusion in apatite gave 760 °C. Type 3 has a range of temperature between 610 and 690 °C, because the exsolved dolomite is too small to identify or the calcite is almost devoid of exsolution.

CARBON ISOTOPE GEOTHERMOMETRY

The temperature dependence of ^{12}C and ^{13}C exchange between calcite and graphite, and dolomite and graphite is an important index of metamorphic temperature in marbles (Valley, 2001). It has been investigated by theoretical (Bottinga, 1969), experimental (e.g. Chacko *et al*., 1991) and empirical methods (e.g. Wada & Suzuki, 1983; Dunn & Valley, 1992). Several studies have shown that calcite–graphite thermometry is a reliable means of estimating the peak metamorphic temperature conditions in marbles (e.g. Dunn & Valley, 1992; Satish-Kumar & Wada, 2000; Satish-Kumar *et al*., 2002; Dunn, 2005).

In this study, two graphite-bearing marble samples which contain Type 1 inclusions were selected for analysis of carbon and oxygen isotope ratios of calcite, dolomite and graphite. The analytical results and fractionations, for respective pairs of calcite–graphite and dolomite–graphite are given in Tables 6 & 7, respectively. The results indicate that the $\delta^{13}C$ values of dolomite are more homogenous than calcite (up to 0.5‰) within a single hand specimen (Table 6).

Table 5. Calcite (Cal)–dolomite (Dol) solvus thermometry results for carbonate inclusions.

Sample no.	Type	Host mineral	Calcite area (pixel)	Dolomite area (pixel)	X_{Mg} (Cal)	X_{Mg} (Dol)	Reintegrated X_{Mg}	Temperature (°C)
116-1-14	Type 2	Spinel	144 214	83 378	0.049	0.477	0.206	870
	Type 2	Forsterite	* electron beam = 50 μm				0.197	855
118-2-18-1	Type 2	Forsterite	280 204	139 440	0.064	0.478	0.202	860
	Type 3	Forsterite	320 823	17 629	0.078	0.482	0.099	670
	Type 3	Forsterite	190 067	26 008	0.077	–	–	620
	Type 3	Forsterite	248 628	61 059	0.076	–	–	610
118-2-18-2	Type 2	Apatite	284 184	75 910	0.056	0.460	0.141	760
119-2-3-1	Type 2	Forsterite	270 972	128 210	0.068	0.468	0.196	855
			* electron beam = 50 μm				0.198	855
	Type 2	Forsterite	267 336	137 250	0.051	0.472	0.194	850
			* electron beam = 50 μm				0.197	855
119-2-3-2	Type 3	Forsterite	239 771	23 508	0.070	0.471	0.106	690
	Type 2	Spinel	211 251	97 556	0.066	0.466	0.192	850
120-1-1 (8)	Type 1	Forsterite	143 368	148 347	0.065	0.472	0.272	970
	Type 1	Forsterite	42 757	60 230	0.067	0.468	0.302	1020
	Type 1	Forsterite	39 (manual)	37 (manual)	0.079	0.482	0.275	980
				Average Type 2 (excluding apatite)				860 ± 8

Table 6. Carbon and oxygen isotopic compositions of calcite, dolomite and graphite.

Sample no.	Mineral				
	Calcite		Dolomite		Graphite
	$\delta^{13}C_{PDB}$	$\delta^{18}O_{SMOW}$	$\delta^{13}C_{PDB}$	$\delta^{18}O_{SMOW}$	$\delta^{13}C_{PDB}$
120-1-1-cc-1	0.22	17.25			
120-1-1-cc-2	0.68	17.49			
119-1-6-cc-3	0.71	18.25			
119-1-6-cc-4	0.47	17.77			
119-1-6-cc-5	0.53	17.99			
120-1-1-dol-6			1.40	20.06	
120-1-1-dol-7			1.24	19.79	
120-1-1-dol-8			1.25	19.82	
119-1-6-dol-9			0.77	18.74	
119-1-6-dol-10			0.80	18.59	
119-1-6-gr-A					−3.15
119-1-6-gr-B					−2.47
119-1-6-gr-C					−2.35
120-1-1-gr-A					−1.35
120-1-1-gr-B					−1.50
120-1-1-gr-C					−1.58

Furthermore, the $\delta^{18}O$ values are more scattered for calcite than dolomite, which indicates the possibility of retrograde interaction with fluids (e.g. Satish-Kumar *et al.*, 1998, 2006a). Textural features also indicate that calcite formed by retrograde reactions and therefore may not be in carbon isotope equilibrium with graphite. Thus, dolomite–graphite fractionations are more consistent among the samples than that of calcite–graphite. These fractionations translate to temperatures of 850 and 810 °C (± 20 °C) with dolomite–graphite thermometry, and 760 and 830 °C for calcite–graphite thermometry were estimated for the two samples using the calibration of Wada & Suzuki (1983; Table 7).

CRYSTAL PREFERRED ORIENTATION OF DOLOMITE LAMELLAE

Crystallographic preferred orientations of host calcite and unmixed dolomite were measured for 18 grains using EBSD. The results show that most of the unmixed dolomite crystals have same crystal preferred orientation to that of the host grain (Fig. 9). Although there is considerable variation in the shape of the exsolved lamellae within a single calcite grain, no relation between shape preferred orientation and crystal preferred orientation could be observed.

In addition, orientation mapping of the matrix calcite exhibiting exsolution textures shows the presence of sub-grain boundaries that separate distinct zones of unmixing (Fig. 10). This texture suggests that the unmixing was after the formation of sub-grains. EBSD results helped to distinguish the sub-grains, which should have been impossible under an optical microscope or even with BSE images.

The CPO of calcite and dolomite in Type 1 inclusions were also measured, which indicated same orientation for both dolomite and calcite (Fig. 9e). This suggests that the unmixing in calcite occurred after its entrapment.

Table 7. Results of carbon isotope geothermometry using the calibration of Wada & Suzuki (1983).

Sample no.	$\delta^{13}C_{PDB}$ (‰)			Fractionations (‰)		Temperature (°C)	
	Calcite	Dolomite	Graphite	$\Delta^{13}C_{Cal\text{-}Gr}$	$\Delta^{13}C_{Dol\text{-}Gr}$	Calcite[a]	Dolomite[a]
120-1-1 (11)	0.68 (1 point)	1.29 ± 0.09 (3 points)	−1.48 ± 0.12 (3 grains)	2.2 ± 0.1	2.8 ± 0.2	830 ± 10	850 ± 20
119-1-6	0.57 ± 0.13 (3 points)	0.78 (2 points)	−2.40 (2 grains)	3.0 ± 0.1	3.2	760 ± 20	810

[a]From Wada & Suzuki.

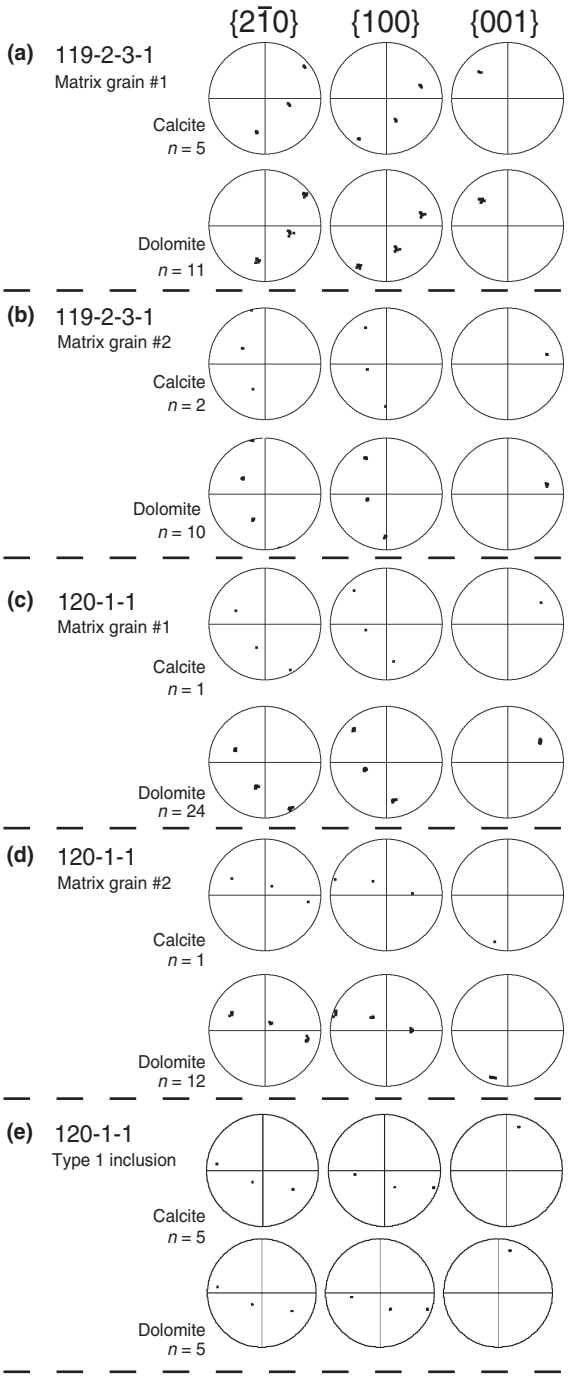

Fig. 9. Comparisons of crystallographic orientations between calcite and dolomite lamellae in four representative grains. Equal areas of lower hemisphere projections of {2–10}, {100} and {001}, respectively. *N* is the number of measured grains. Note that each pair of calcite and unmixed dolomite shows the same orientation.

DISCUSSION

Interpretation of calcite–dolomite solvus temperatures

Recently, numerous researchers have applied calcite–dolomite solvus thermometry to estimate the metamorphic temperatures in high-grade marbles (Dunn, 2005; Müller *et al.*, 2008 and references therein). However, accurate estimation is hindered by the presence of large variations in X_{Mg} values. Earlier studies proposed that the highest measured X_{Mg} value can be potentially used for the estimation of peak metamorphic temperatures, assuming that the lower X_{Mg} values are because of retrograde re-equilibration (Holness *et al.*, 1991; Masch & Heuss-Abichler, 1991; Cook & Bowman, 1994). This method will not work in the case of high-grade marbles because of the extensive development of unmixed lamellae. A possible solution is to reintegrate unmixed dolomite with the host calcite to infer the peak metamorphic temperatures. Again there are limitations here as well, and hence calcite–dolomite solvus geothermometer for high-grade marbles has less reliability for understanding the peak metamorphic conditions. However, Ogasawara *et al.* (1998) and Ferry (2001) estimated the temperature of metamorphism (retrograde ultra high pressure metamorphism and peak contact metamorphism, respectively) using high magnesian calcite inclusions within silicate minerals. Their results indicate that calcite inclusions have higher X_{Mg} compared with matrix calcite, and can be adopted for an estimation of peak metamorphic temperature.

In this study, a significant difficulty encountered in the reintegration and temperature estimation for inclusions is that different cross-sections through a heterogeneously distributed dolomite exsolution will give varying temperature (Table 5). Although EBSD results of two Type 1 inclusions indicated unmixing of calcite and dolomite from a single phase, these inclusions are more likely to have heterogeneous distribution of dolomite because of the 'cut effect'. Thus, the relative area of calcite and dolomite is strongly affected by the cut effect, which produces large uncertainties in temperature estimates. The extreme case of this cut effect is found as Type 3 inclusions, consisting of either dolomite or calcite, which might be a part of a Type 1 inclusion in three dimensions. Therefore, it is suggested that Types 1 and 3 are not suited for the reintegration of calcite composition at the time of entrapment. However, Type 2 inclusions have relatively homogeneous unmixing of dolomite and therefore can be more reliably reintegrated. Six Type 2 inclusions in forsterite and spinel gave similar reintegrated temperatures (860 ± 8 °C). These results are similar to the temperature estimated by dolomite–graphite carbon isotope geothermometer and fall within the range of temperature estimates reported in Yoshimura *et al.* (2004). One Type 2 inclusion in apatite yielded 760 °C, which suggests an early stage formation of apatite compared with forsterite and spinel during prograde metamorphism.

Therefore, calcite–dolomite solvus geothermometry results obtained in this study using carbonate inclusions in apatite possibly record prograde temperatures, whereas those in forsterite and spinel correspond to

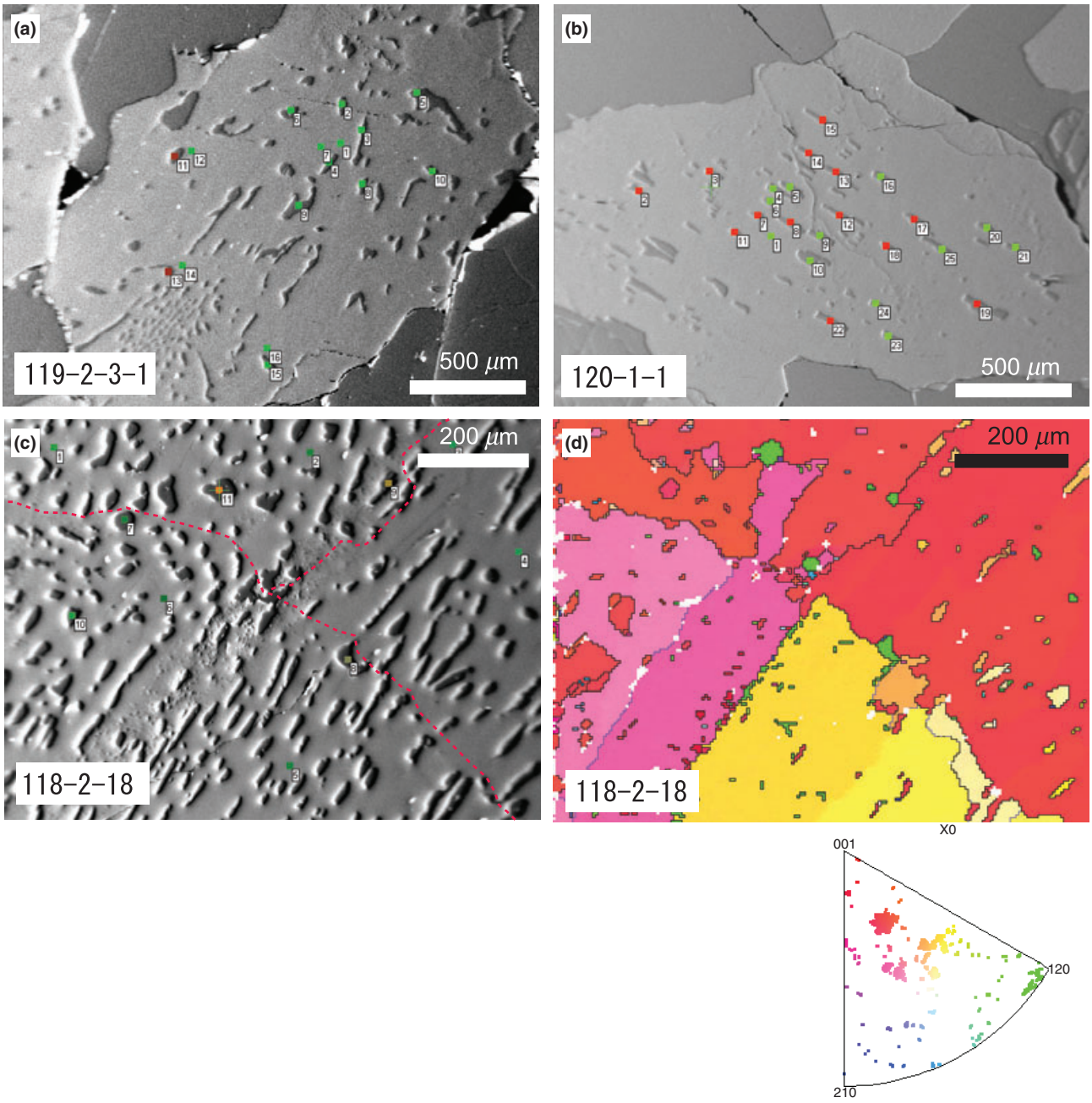

Fig. 10. (a) Backscattered electron image (BSE) of matrix calcite showing the distribution of dolomite lamellae and sub-grain boundary of calcite. The green (host) and red (lamellae) filled squares with numbers indicate analytical points where orientations were determined using EBSD. (b) Distribution of elongated dolomite lamellae in calcite along with fine-grained lamellae. (c) BSE image of matrix calcite showing different morphologies of elongated tabular and spherical grains of dolomite unmixing. The red dashed lines show the grain boundary recognized by the polarized microscope. (d) EBSD orientation map of calcite showing exsolution texture. The mapped area is the same as that in (c). Different colours correspond to different crystallographic orientations. Note the occurrence of sub-grain boundaries. The white regions are the vacant spaces and the blue or green are the dolomite lamellae.

peak metamorphic temperature. These temperatures match well with those reported for the regional granulite facies metamorphism in the LHC (Motoyoshi & Ishikawa, 1997; Satish-Kumar & Wada, 2000; Yoshimura *et al.*, 2004). In contrast, matrix calcite gave lower temperature estimates, even after reintegration of exsolved dolomite (720–760 °C), corresponding to retrograde metamorphic conditions. Several stages of retrograde metamorphic events have been proposed in the LHC (see Satish-Kumar *et al.*, 2010 and references therein). Our temperature estimates based on calcite–dolomite solvus thermometry are in agreement with

the retrograde *P–T* estimates of Ikeda (2004) based on garnet–biotite thermometry. The possible temperature conditions of different stages of the metamorphic *P–T* path for the Skallevikshalsen region estimated from different independent estimates, including those from this study are shown in Fig. 11.

Merits and limitations of 'carbonate inclusion' geothermometry

The merit of using carbonate inclusions for the estimation of peak metamorphic temperature is that the influence of re-equilibration of Mg during retrograde metamorphism can be avoided. However, calcite inclusions in high-grade marbles occur in different shapes, sizes and display various unmixing features. Such variations in unmixing imply that the inclusions can be trapped during various stages of formation of its host mineral. Consequently, the integrated X_{Mg} values of inclusions may give lower temperatures than the peak metamorphic conditions. However, careful selection of inclusions with negative crystal shapes, and homogenous unmixing textures help in estimating peak metamorphic temperatures.

Inconsistencies in the estimation of temperatures using calcite inclusion can also result from the heterogeneous distribution of unmixed dolomite, which has to be evaluated before the application of solvus thermometry. For example, the overestimated temperature for Type 1 inclusion was caused by the irregular morphology of the unmixed dolomite. In addition, proper estimation of the calcite–dolomite ratio can be difficult if the exsolution is fine-grained and inclusions are very small. The presence of submicroscopic lamellae also influences analysis of chemical composition and integration of area (e.g. Müller *et al.*, 2008). A comparison of reintegration using digital images and focused beam analyses, and broad beam analyses gave similar results for fine-grained exsolution (see Table 5) and hence our results were not affected by submicroscopic lamellae.

Implications for calcite–dolomite unmixing

Minerals that form solid solutions, such as carbonate, feldspar or pyroxene, may adjust to lower temperature at certain conditions by unmixing (Putnis, 1992). This results in microstructures that grow at conditions where the host mineral becomes thermodynamically less stable than a mixture of two minerals that have closely related structures to the original host. Such microstructures contain information regarding non-equilibrium thermodynamics that can possibly be utilized to infer pressure, temperature, deformation and material properties. Kuhl & Schmid (2007) suggested a simulation model for mineral growth during unmixing governed by the classical Cahn–Hilliard equation. Their model builds up on related work in polymer and metallurgical science where the evolution of exsolution phenomena is described by an early stage of phase separation and late stage of Ostwald ripening. They also derived a formulation which can predict the formation of both particulate and worm-like microstructures during unmixing in response to varying initial composition. In addition, the crystallographic preferred orientation of the unmixed phase has resulted from the anisotropy in diffusion coefficients and that the preferential orientation is orthogonal to the fast diffusion direction. Microstructural and crystallographic data in this study indicates that the coarse

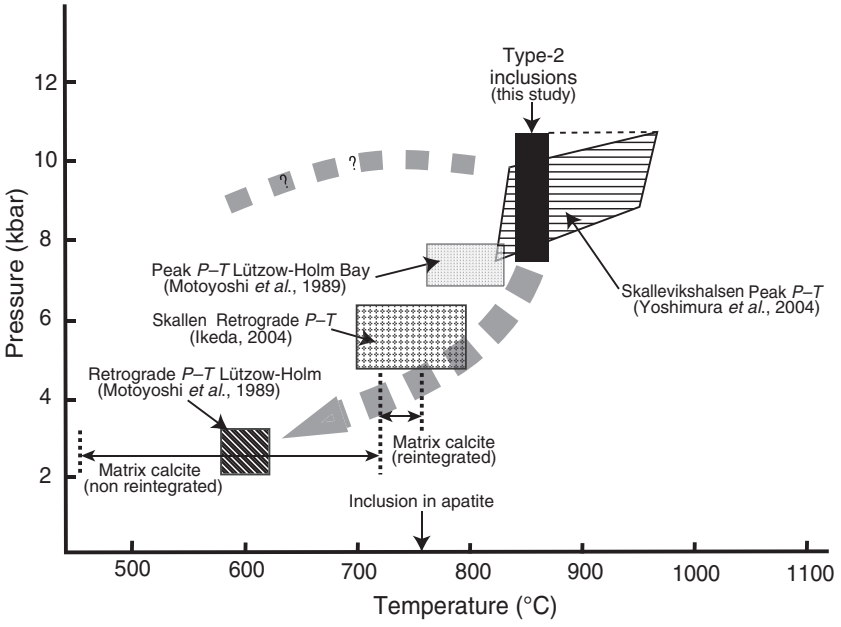

Fig. 11. Summary of metamorphic *P–T* evolution history deduced from the Skallevikshalsen region in Lützow-Holm Complex, East Antarctica. Calcite–dolomite solvus geothermometric results (black vertical lines) were estimated using calcite inclusions from marbles. These results are compared with the reported peak metamorphic *P–T* conditions in Skallevikshalsen. Note that the integrated temperatures of Type 2 inclusions are similar to the peak temperature estimates using metapelitic rocks by Yoshimura *et al.* (2004). Type 3 inclusions might have been included during the prograde growth of forsterite. Reintegrated matrix calcite yielded temperature of ~750 °C whereas non-reintegrated matrix calcite yielded temperature of ~560 ± 40 °C. Calcite–dolomite solvus thermometry results matches with the existing *P–T* evolution of the terrane (Motoyoshi *et al.*, 1989).

tabular dolomite lamellae in Skallevikshalsen marbles were possibly formed by the anisotropic diffusion of Mg. The progressive shape change from particulate or fine wormy lamellae to larger tabular lamellae is also controlled by interfacial energy (Toriumi, 1987; Okamoto & Michibayashi, 2005).

The result of crystallographic orientation mapping of matrix calcite using the EBSD shows development of sub-grains to both sides of a grain boundary (compare Fig. 10c with d). This microstructure implies that grain boundary fluids may have played a prominent role in the formation of sub-grains. Earlier studies using stable isotopes have shown that the marbles at LHC have been subjected to multiple stages of fluid infiltration (Satish-Kumar *et al.*, 1998, 2006a, 2010). Dissolution and re-precipitation is a common phenomenon that can easily re-equilibrate calcite. Dolomite exsolution in the sub-grain calcite is very fine-grained and wormy. The presence of grain boundary fluids or late deformation might have driven recrystallization that produced the sub-grains with fine-grained dolomite lamellae. Although it is difficult to distinguish the boundary between grain and sub-grain by petrography or even with BSE images, crystal orientation maps helped in identifying the development of sub-grains (Fig. 9d). Therefore, an evaluation of the EBSD pattern of dolomite lamellae and the host would help in accurate estimation of metamorphic temperatures using calcite–dolomite solvus geothermometry in high-grade marbles. The misorientation of dolomite grains are considered as preexisting ones and can be excluded during reintegration of composition.

The EBSD results (18 grains) of host matrix calcite core and dolomite lamellae (Fig. 9) indicate that the unmixed dolomite is crystallographically oriented parallel to the direction of the host calcite (Fig. 10a,b). This tendency implies that dolomite grew in the same orientation as that of the host calcite. Putnis (1992) suggested that the shape and orientation of the unmixed phase will be controlled by the elastic anisotropy of the host phase such that interfacial energy and strain energy are minimizing. Most exsolved dolomite has CPO patterns close to the host crystals, suggesting similar elastic properties for both calcite and dolomite. However, few CPO data (two grains) show unusual patterns; the crystallographic orientations of dolomite lamellae do not correspond to those of host calcite. The reasons for such exceptions have not been understood yet, which needs further detailed studies. There is a possibility that the elastic and energy controls were overcome by the supersaturation of Mg in the host calcite.

In this study, the chemical composition (Ca and Mg content) of the calcite matrix does not exhibit systematic zoning patterns such as those reported by Wada & Suzuki (1983) in the contact aureole of Kasuga (Japan). The absence of zoning patterns can be attributed to higher temperature and/or longer crustal residence time of marbles during regional metamorphism in continental collisional tectonic setting. Experimental study of cation diffusion in carbonate minerals suggest that if temperatures are hot and/or the duration is long enough, then the cation diffusion will homogenize any chemical heterogeneities (Fisler & Cygan, 1998).

CONCLUSIONS

Carbonate mineral inclusions within refractory minerals such as forsterite, spinel and apatite in high-grade marbles are potential candidates for an estimation of peak metamorphic temperature. Careful selection of inclusions is essential for successfully retrieving the composition of calcite at the time of entrapment. 'Negative crystal' shapes, homogenous exsolution textures and isolation from matrix carbonate are important criteria to select the inclusions. At Skallevikshalsen, East Antarctica, a narrow range of metamorphic temperatures were estimated (850–870 °C) from carbonate inclusions, which is consistent with the dolomite–graphite carbon isotope geothermometer and the existing temperature estimates using cation-exchange geothermometers. The matrix calcite and dolomite lamellae have the same crystallographic preferred orientations suggesting that the growth of exsolution lamellae is controlled by the anisotropy of the diffusion coefficients.

ACKNOWLEDGEMENTS

The authors gratefully acknowledge H. Wada for insightful and constructive comments in this study, T. Tsunogae for assistance with the analysis of halogen content at University of Tsukuba, Japan, and M. Muramoto for help with EBSD (Shizuoka University, Japan). Important advice about carbonate inclusions and morphology of unmixed lamellae was received from E. Essene and A. Putnis, which helped a great deal in the progress of this study. Critical and constructive review comments from E. Essene, S. Dunn and A. Okamoto helped in improving the manuscript considerably. The authors thank D. Robinson for his editorial comments. The marble samples from Skallevikshalsen were collected during JARE-46, and M. Satish-Kumar thanks the geological group for support in the field. Part of this study was supported by National Institute of Polar Research (Project-7 led by Y. Motoyoshi). This study was supported by the grant-in-aid for young scientist (nos 18740319 and 20684022) to M. Satish-Kumar from the Ministry of Education, Culture, Sports, Science and Technology, Japan (Mombukagakusho).

REFERENCES

Anovitz, L.M. & Essene, E.J., 1987. Phase equilibria in the system $CaCO_3$-$MgCO_3$-$FeCO_3$. *Journal of Petrology*, **28,** 389–414.

Bence, A.E. & Albee, A.L., 1968. Empirical correction factors for the electron microanalysis of silicates and oxides. *Journal of Geology*, **76,** 382–403.

Bohlen, S.R., 1987. Pressure–temperature–time paths and a tectonic model for the evolution of granulites. *Journal of Geology*, **95,** 617–632.

Bottinga, Y., 1969. Calculated fractionation factors for carbon and hydrogen isotope exchange in the system calcite-carbon dioxide-graphite-methane-hydrogen-water vapor. *Geochimica et Cosmochimica Acta*, **33,** 49–64.

Buddington, A.F. & Lindsley, D.H., 1964. Iron-titanium oxide minerals and synthetic equivalents. *Journal of Petrology*, **5,** 310–357.

Chacko, T., Mayeda, T.K., Clayton, R.N. & Goldsmith, J.R., 1991. Oxygen and carbon isotope fractionations between CO_2 and calcite. *Geochimica et Cosmochimica Acta*, **55,** 2867–2882.

Cook, S.J. & Bowman, J.R., 1994. Contact-metamorphism surrounding the altastock-thermal constraints and evidence of advective heat-transport from calcite plus dolomite geothermometry. *American Mineralogist*, **79,** 513–525.

Dickson, J.A.D., 1965. A modified staining technique for carbonates in thin section. *Nature*, **205,** 587.

Droop, G.T.R. & Al-Filali, I.Y., 1996. Interaction of aqueous fluids with calcareous metasediments during high-T, low-P regional metarmorphism in the Qadda area, southern Arabian Shield. *Journal of Metamorphic Geology*, **14,** 613–634.

Dunn, S.R., 2005. Calcite-graphite isotope thermometry in amphibolite facies marble, Bancroft, Ontario. *Journal of Metamorphic Geology*, **23,** 817–827.

Dunn, S.R. & Valley, J.W., 1992. Calcite-graphite isotope thermometry: a test for polymetamorphism in marble, Tudor gabbro aureole, Ontario, Canada. *Journal of Metamorphic geology*, **10,** 487–501.

Essene, E.J., 1982. Geologic thermometry and barometry. *Reviews in Mineralogy*, **10,** 153–206.

Ferry, J.M., 2001. Calcite inclusions in forsterite. *American Mineralogist*, **86,** 773–779.

Fisler, D.K. & Cygan, R.T., 1998. Cation diffusion in calcite: determining closure temperatures and the thermal history for the ALH84001 meteorite. *Meteoritics and Planetary Science*, **33,** 785–789.

Fitzsimons, I.C.W. & Harley, S.L., 1995. Garnet coronas in scapolite-wollastonite calc-silicates from East Antarctica: the application and limitations of activity-corrected grids. *Journal of Metamorphic Geology*, **12,** 761–777.

Fraser, G., McDougall, I., Ellis, D.J. & Williams, I.S., 2000. Timing and rate of isothermal decompression in Pan-African granulites from Rundvågshetta, East Antarctica. *Journal of Metamorphic Geology*, **18,** 441–454.

Goldsmith, J.R. & Newton, R.C., 1969. P–T–X relations in the system $CaCO_3$-$MgCO_3$ at high temperatures and pressures. *American Journal of Science*, **267A,** 160–190.

Harley, S.L., 1989. The origin of granulites: a metamorphic perspective. *Geological Magazine*, **126,** 215–247.

Hess, H.H., 1960. Stillwater igneous complex, Montana – a quantitative mineralogical study. *Geological Society of America Memoir*, **80,** 230 pp.

Hiroi, Y., Shiraishi, K. & Motoyoshi, Y., 1991. Late Proterozoic paired metamorphic complexes in East Antarctica, with special reference to the tectonic significance of ultramafic rocks. In: *Geological Evolution of Antarctica* (eds Thompson, M.R.A., Crame, J.A. & Thompson, J.W.), pp. 83–87. Cambridge University Press, Cambridge.

Hokada, T. & Motoyoshi, Y., 2006. Electron microprobe technique for U-Th-Pb and REE chemistry of monazite, and its implications for pre-, peak- and postmetamorphic events of the Lützow-Holm Complex and the Napier Complex, East Antarctica. *Polar Geoscience*, **19,** 118–151.

Holness, M.B., Bickle, M.J. & Graham, C.M., 1991. On the kinetics of textural equilibration in forsterite marbles. *Contributions to Mineralogy and Petrology*, **108,** 356–367.

Ikeda, T., 2004. Garnet-biotite thermometry of a pelitic gneiss from the Lützow-Holm Complex in Skallen, East Antarctica: constraints on retrograde metamorphism. *Polar Geoscience*, **17,** 45–57.

Jacobs, J. & Thomas, R.J., 2004. A Himalayan-type indenter-escape tectonic model for the southern part of the Late Neoproterozoic Early Paleozoic East African-Antarctic Orogen. *Geology*, **32,** 721–724.

Jaffe, H.W., Robinson, P. & Tracy, R.J., 1975. Orientation of pigeonite exsolution lamellae in metamorphic augite: correlation with composition and calculated optimal phase boundaries. *American Mineralogist*, **60,** 9–28.

Kawakami, T. & Ikeda, T., 2004. Timing of ductile deformation and peak metamorphism in Skallevikshalsen, Lützow-Holm Complex, East Antarctica. *Polar Geoscience*, **17,** 1–11.

Kretz, R., 1983. Symbols for rock-forming minerals. *American Mineralogist*, **68,** 277–279.

Kretz, R., 1988. SEM study of dolomite microcrystals in Grenville marble. *American Mineralogist*, **73,** 619–631.

Kuhl, E. & Schmid, D.W., 2007. Computational modeling of mineral unmixing and growth. An application of the Cahn–Hilliard equation. *Computational Mechanics*, **39,** 439–451.

Letargo, C.M.R., Lamb, W.M. & Park, J.S., 1995. Comparison of calcite + dolomite thermometry and carbonate + silicate equilibria: constraints on the conditions of metamorphism of the Llano uplift, central Texas, U.S.A. *American Mineralogist*, **80,** 131–143.

Masch, L. & Heuss-Abichler, S., 1991. Decarbonation reactions in siliceous dolomites and impure limestones. In: *Equilibrium and Kinetics in Contact Metamorphism. The Ballachulish Igneous Complex and its Aureole* (eds Voll, G., Topel, J., Pattison, D.R.M. & Seifet, F.), pp. 211–227. Springer, New York.

Motoyoshi, Y. & Ishikawa, M., 1997. Metamorphic and structural evolution of granulites from Rundvågshetta, Lützow-Holm Bay, East Antarctica. In: *The Antarctic Region: Geological Evolution and Processes* (ed. Ricci, C.A.), pp. 65–72. Terra Antarctic Publications, Siena.

Motoyoshi, Y., Matsubara, S. & Matsueda, H., 1989. P–T evolution of the granulite facies rocks of the Lutzow-Holm Bay region, East Antarctica. In: *Evolution of Metamorphic Belts* (eds Daly, J.S., Cliff, R.A. & Yardley, B.W.D.), Geological Society of London, Special Publication, **43,** 325–329.

Müller, T., Baumgartner, L.P., Foster, C.T. & Roselle, G.T., 2008. Forward modeling of the effects of mixed volatile reaction, volume diffusion, and formation of submicroscopic exsolution lamellae on calcite-dolomite thermometry. *American Mineralogist*, **93,** 1245–1259.

Nakamura, Y. & Kushiro, I., 1970. Equilibrium relations of hypersthene, pigeonite and augite in crystallizing magmas: microprobe study of a pigeonite andesite from Weiselbelg, Germany. *American Mineralogist*, **55,** 1999–2015.

Ogasawara, Y., Zhang, R.Y. & Liou, J.G., 1998. Petrogenesis of dolomitic marbles from Rongcheng in the Su-Lu ultrahigh-pressure metamorphic terrane, eastern China. *The Island Arc*, **7,** 82–97.

Okamoto, A. & Michibayashi, K., 2005. Progressive shape evolution of a mineral inclusion under differential stress at high temperature: example of garnet inclusions within a granulite-facies quartzite from the Lützow-Holm Complex, East Antarctica. *Journal of Geophysical Research*, **110,** B11203; doi: 10.1029/2004JB003526.

Pattison, D.R.M., Chacko, T., Farquhar, J. & McFarlane, C.R.M., 2003. Temperatures of granulite-facies metamorphism: constraints from experimental phase equilibria and thermobarometry corrected for retrograde exchange. *Journal of Petrology*, **44,** 867–900.

Perkins, D., Essene, E.J. & Marcotty, L.A., 1982. Thermometry and barometry of some amphibolite-granulite facies rocks from the Otter Lake area, southern Quebec. *Canadian Journal of Earth Science*, **19,** 1759–1774.

Piazolo, S. & Markl, G., 1999. Humite- and scapolite-bearing assemblages in marbles and calcsilicates of Dronning Maud Land, Antarctica: new data for Gondwana reconstructions. *Journal of Metamorphic Geology*, **17,** 91–107.

Powell, R. & Holland, T.J.B., 2001. Course Notes for 'THERMOCALC Workshop 2001: Calculating Metamorphic Phase Equilibria' (on CD-ROM).

Powell, R., Condcliffe, D.M. & Condcliffe, E., 1984. Calcite-dolomite geothermometry in the system $CaCO_3$-$MgCO_3$-$FeCO_3$: an experimental study. *Journal of Metamorphic Geology*, **2,** 33–41.

Proyer, A., Mposkos, E., Baziotis, I. & Hoinkes, G., 2008. Tracing high-pressure metamorphism in marbles: phase relations in high-grade aluminous calcite–dolomite marbles from the Greek Rhodope massif in the system CaO–MgO–Al_2O_3–SiO_2–CO_2 and indications of prior aragonite. *Lithos*, **104,** 119–130.

Putnis, A., 1992. *Introduction to Mineral Sciences*. Cambridge University Press, London.

Robinson, P., Ross, M., Nord, G.L., Smyth, J.R. & Jaffe, H.W., 1977. Exsolution lamellae in augite and pigeonite: fossil indicators of lattice parameters at high temperature and pressure. *American Mineralogist*, **62,** 857–873.

Satish-Kumar, M. & Wada, H., 2000. Carbon isotopic equilibrium between calcite and graphite in Skallen Marbles, East Antarctica: evidence for the preservation of peak metamorphic temperatures. *Chemical Geology*, **166,** 173–182.

Satish-Kumar, M., Yoshida, M., Wada, H., Niitsuma, N. & Santosh, M., 1998. Fluid flow along micro-fractures in calcite marbles from east Antarctica: evidence from gigantic (21‰) oxygen isotopic zonation. *Geology*, **26,** 251–254.

Satish-Kumar, M., Wada, H., Santosh, M. & Yoshida, M., 2001. Fluid-rock history of granulite facies humite-marbles from Ambasamudram, southern India. *Journal of Metamorphic Geology*, **19,** 395–410.

Satish-Kumar, M., Wada, H. & Santosh, M., 2002. Constraints on the application of carbon isotope thermometry in high- to ultrahigh-temperature metamorphic terranes. *Journal of Metamorphic Geology*, **20,** 335–350.

Satish-Kumar, M., Hermann, J., Tsunogae, T. & Osanai, Y., 2006a. Carbonation of Cl-rich scapolite boudins in Skallen, East Antarctica: evidence for changing fluid condition in the continental crust. *Journal of Metamorphic Geology*, **24,** 241–261.

Satish-Kumar, M., Mori, H., Kusachi, I. & Wada, H., 2006b. Cathodoluminescence microscopy of high-temperature skarn minerals from Fuka contact aureole, Okayama, Japan. *Geoscience Reports of Shizuoka University*, **33,** 21–28.

Satish-Kumar, M., Hokada, T., Kawakami, T. & Dunkley, D.J., 2008a. Geosciences research in East Antarctica: present status and future perspectives. In: *Geodynamic Evolution of East Antarctica: A Key to the East–West Gondwana Connection* (eds Satish-Kumar, M., Motoyoshi, Y., Osanai, Y., Hiroi, Y. & Shiraishi, K.), Geological Society of London, Special Publications, **308,** 1–21.

Satish-Kumar, M., Miyamoto, T., Hermann, J., Kagami, H., Osanai, Y. & Motoyoshi, Y., 2008b. Pre-metamorphic carbon, oxygen and strontium isotope signature of high-grade marbles from the Lützow Holm Complex, East Antarctica: apparent age constraints of carbonate deposition. In: *Geodynamic Evolution of East Antarctica: A Key to the East–West Gondwana Connection* (eds Satish-Kumar, M., Motoyoshi, Y., Osanai, Y., Hiroi, Y. & Shiraishi, K.), Geological Society of London, Special Publications, **308,** 147–164.

Satish-Kumar, M., Hermann, J., Miyamoto, T. & Osanai, Y., 2010. Fingerprinting a multistage metamorphic fluid-rock history: evidence from grain scale Sr, O and C isotopic and trace element variations in high-grade marbles from East Antarctica. *Lithos*, **114,** 217–228.

Schmidt, N.H. & Olesen, N.O., 1989. Computer-aided determination of crystal lattice orientation from electron channeling patterns in the SEM. *Canadian Mineralogist*, **27,** 15–22.

Seto, Y., Ohi, S., Shimobayashi, N. *et al.*, 2006. Clinopyroxene exsolution in wollastonite from Namaqualand granulite, South Africa. *American Mineralogist*, **91,** 446–450.

Shiraishi, K., Hiroi, Y. & Motoyoshi, Y., 1989. *Geological Map of Lützow-Holm Bay, Antarctica. Antarctic Geological Map Series Sheet 12*. National Institute of Polar Research, Tokyo.

Shiraishi, K., Ellis, D.J., Hiroi, Y., Fanning, C.M., Motoyoshi, Y. & Nakai, Y., 1994. Cambrian orogenic belt in East Antarctica and Sri Lanka: implications for Gondwana assembly. *Journal of Geology*, **102,** 47–65.

Shiraishi, K., Dunkley, D.J., Hokada, T., Fanning, C.M., Kagami, H. & Hamamoto, T., 2008. Geochronological constraints on the Late Proterozoic to Cambrian crustal evolution of eastern Dronning Maud Land, East Antarctica: a synthesis of SHRIMP U-Pb age and Nd model age data. In: *Geodynamic Evolution of East Antarctica: A Key to the East–West Gondwana Connection* (eds Satish-Kumar, M., Motoyoshi, Y., Osanai, Y., Hiroi, Y. & Shiraishi, K.), Geological Society Special Publication, **308,** 21–67.

Spear, F.S., 1993. Metamorphic phase equilibria and pressure–temperature–time paths. *Mineralogical Society of America Monograph Series*, **1,** 799 pp.

Toriumi, M., 1987. Progressive deformation and annealing of quartz inclusion in porphyroblastic feldspar during synmetamorphic non-coaxial deformation. *Journal of Japanese Association for Mineralogists, Petrologists and Economic Geologists*, **82,** 123–131.

Valley, J.W., 2001. Stable isotope thermometry. In: *Stable isotope geochemistry* (eds Valley, J.W. & Cole, D.R.), *Reviews in Mineralogy and Geochemistry*, **43,** 365–413.

Wada, H. & Suzuki, K., 1983. Carbon isotope thermometry calibrated by dolomite-calcite solvus temperatures. *Geochimica et Cosmochimica Acta*, **47,** 697–706.

Wada, H., Fujii, N. & Niitsuma, N., 1984a. Analytical method of stable isotope for ultra-small amounts of carbon dioxide with MAT-250 mass spectrometer. *Geoscience Reports of Shizuoka University*, **10,** 103–112.

Wada, H., Ito, R. & Akiyama, F., 1984b. Preparation and measurement of carbon dioxide for stable isotope analysis of small amount of graphite. *Geoscience Reports of Shizuoka University*, **10,** 133–141.

Yoshida, M., Yoshida, Y., Ando, H., Ishikawa, T. & Tatsumi, T., 1976. *Explanatory Text of Geological Map of Skallen, Antarctica, Antarctic Geological Map Series Sheet 9 Skallen*. National Institute of Polar Research, Tokyo.

Yoshimura, Y., Motoyoshi, Y., Miyamoto, T., Grew, E.S., Carson, C.J. & Dunkley, D.J., 2004. High-grade metamorphic rocks from Skallevikshalsen in the Lützow-Holm Complex, East Antarctica: metamorphic conditions and possibility of partial melting. *Polar Geoscience*, **17,** 57–87.

Received 5 November 2009; revision accepted 31 March 2010.